Interaction between Stray Electrostatic Fields and a Charged Free-Falling Test Mass

F. Antonucci,[1] A. Cavalleri,[2] R. Dolesi,[1] M. Hueller,[1] D. Nicolodi,[1] H. B. Tu,[1] S. Vitale,[1] and W. J. Weber[1]

[1]*Dipartimento di Fisica, Università di Trento, and I.N.F.N., Gruppo di Trento, 38123 Povo (TN), Italy*

[2]*Istituto di Fotonica e Nanotecnologie, C.N.R.- Fondazione Bruno Kessler, 38123 Povo (TN), Italy*

(Received 3 December 2011; published 30 April 2012)

We present an experimental analysis of force noise caused by stray electrostatic fields acting on a charged test mass inside a conducting enclosure, a key problem for precise gravitational experiments. Measurement of the average field that couples to the test mass charge, and its fluctuations, is performed with two independent torsion pendulum techniques, including direct measurement of the forces caused by a change in electrostatic charge. We analyze the problem with an improved electrostatic model that, coupled with the experimental data, also indicates how to correctly measure and null the stray field that interacts with the test mass charge. Our measurements allow a conservative upper limit on acceleration noise, of 2 $(\mathrm{fm/s^2})/\mathrm{Hz^{1/2}}$ for frequencies above 0.1 mHz, for the interaction between stray fields and charge in the LISA gravitational wave mission.

DOI: 10.1103/PhysRevLett.108.181101 PACS numbers: 04.80.Nn, 07.87.+v, 41.20.Cv, 91.10.Pp

Limiting stray forces on a test mass (TM) is crucial for precise experimental gravitation, from gravitational wave observation [1–3] to tests of the equivalence principle [4], short range gravity [5,6], and relativistic gyroscope precession [7,8]. In all these experiments, electrostatic force noise is cited as a precision-limiting effect.

The orbiting gravitational wave observatory LISA (Laser Interferometry Space Antenna [3]) requires, along its sensitive x axis, free fall to within 3 $(\mathrm{fm/s^2})/\mathrm{Hz^{1/2}}$ residual acceleration—6 $\mathrm{fN/Hz^{1/2}}$ force noise—at frequencies 0.1–3 mHz. For LISA and its precursor LISA Pathfinder [9,10], the TM is a 46 mm gold-coated cube inside a co-orbiting satellite and shielded, without mechanical contact, by the gold-coated surfaces of a capacitive position sensor [11,12], which can also apply actuation voltages.

While the sensor is nominally an equipotential shield, two factors can produce electrostatic forces relevant at the femtonewton level. First, the floating TM accumulates charge from cosmic and solar particles, with an expected net rate of the order of 50 e/s [13]. Second, real metals display stray potential differences [14,15] between different points on a single conducting surface. These arise in different exposed crystalline facets and surface contamination. Typical observed average potential differences between roughly centimeter-size regions of a gold surface are of the order of 10–100 mV [16–19].

By itself, TM charge q creates a force gradient coupling to spacecraft motion, requiring periodic discharge [20]. Stray potentials δV also create force gradients, whose d^{-3}—or stronger [21]—dependence on the TM-sensor gap d, motivates large, several millimeter, gaps for LISA. Fluctuations in δV also create force noise.

The mutual interaction between charge and stray potentials [22–25] can be written, to linear order in q,

$$F_x = -\frac{q}{C_T}\left|\frac{\partial C_X}{\partial x}\right|\Delta_x. \tag{1}$$

Δ_x is an effective potential difference proportional to $\frac{\partial F_x}{\partial q}$ and will be calculated shortly. C_X and C_T are, respectively, the TM capacitances to an X electrode and the entire sensor (see Fig. 1).

This interaction produces force noise in two ways. First, any residual Δ_x multiplies random charge noise:

$$S^{1/2}_{F(\delta q)} = \frac{S^{1/2}_q}{C_T}\left|\frac{\partial C_X}{\partial x}\right|\Delta_x \approx 7\ \mathrm{fN/Hz^{1/2}} \times \left(\frac{\Delta_x}{0.1\ \mathrm{V}}\right)\left(\frac{\lambda_{\mathrm{eff}}}{300/\mathrm{s}}\right)^{1/2}\left(\frac{10^{-4}\ \mathrm{Hz}}{f}\right). \tag{2}$$

$\Delta_x \approx 100$ mV is typical for LISA prototype sensors [16,17,26]. λ_{eff} is the equivalent single charge event rate that gives a "red" Poissonian shot noise $S_q = \frac{2e^2\lambda_{\mathrm{eff}}}{\omega^2}$, estimated at roughly $300/\mathrm{s}$ [13], larger during solar flare events [27]. This random charge force noise $S_{F(\delta q)}$ can be eliminated by nulling Δ_x with applied voltages [16,25].

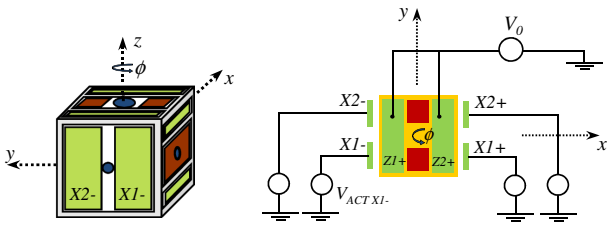

FIG. 1 (color online). Capacitive sensor, including (right) X and Z electrode connections in the Z-modulation experiments. The TM-electrode gaps are 4, 2.9, and 3.5 mm on, respectively, the X, Y, and Z faces. The presented torsion pendulum measurements detect the rotation ϕ.

Second, fluctuations in Δ_x will multiply any nonzero TM charge to produce force noise:

$$S^{1/2}_{F(\delta\Delta_x)} = \frac{q}{C_T}\left|\frac{\partial C_X}{\partial x}\right| S^{1/2}_{\Delta_x} \approx 1.3\ \mathrm{fN/Hz^{1/2}} \times \left(\frac{q}{10^7 e}\right)\left(\frac{S^{1/2}_{\Delta_x}}{100\ \mu\mathrm{V/Hz^{1/2}}}\right). \quad (3)$$

$10^7 e$ is roughly two days of accumulated charge and a reasonable discharge threshold.

This Letter addresses these two sides of the q-δV interaction. Our analysis, considering spatial surface potential variations on both the TM and sensor, highlights systematic errors in measuring Δ_x with applied electrostatic fields, consistent with our experimental data. Force noise from field fluctuations is then addressed by measurements of stray potential fluctuations. Experiments employ a hollow LISA-like TM suspended as a torsion pendulum inside a prototype LISA capacitive sensor connected to a prototype sensing and actuation electronics [16]. All relevant surfaces have been sputtered with gold and held under vacuum for more than a year. Our measurements in this flight-realistic configuration allow a conservative upper limit for the TM acceleration noise caused by the interaction between charge and stray fields.

The electrostatic interaction is modeled as a patchwork of discrete TM and sensor (S) surface domains at potentials V_i (see Fig. 2), coupled by capacitors C_{ij}, with $q_i = \sum_j C_{ij}(V_i - V_j)$ [28]. Stray potentials are defined by ideal generators δV_i. For a sensor domain, $V_i = \delta V_i$ or, if located on an electrode attached to generator $V_{\mathrm{ACT}n}$, $V_i = \delta V_i + V_{\mathrm{ACT}n}$. For a TM domain, $V_i = \delta V_i + V_{\mathrm{TM}}$, where V_{TM} is an effective average TM potential [30]:

$$V_{\mathrm{TM}} = \frac{q}{C_T} + \frac{\sum_{j(S)} C_{Sj} V_j}{C_T}, \quad (4)$$

where index $j(S)$ restricts the sum to sensor domains. $C_{Sj} \equiv \sum_{i(\mathrm{TM})} C_{ij}$ is the total capacitance between sensor domain j and all TM domains, and $C_T \equiv \sum_{j(S)} C_{Sj}$ is the total TM capacitance to the sensor.

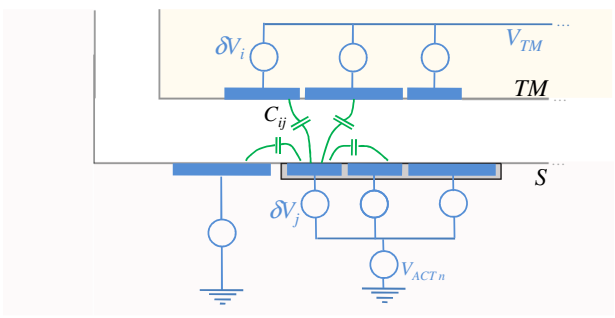

FIG. 2 (color online). Schematic of the electrostatic model, with capacitively coupled sensor (S) and TM domains.

The force on the TM along the x axis is

$$F_x = \frac{1}{2}\sum_{i,j<i}\frac{\partial C_{ij}}{\partial x}(V_i - V_j)^2, \quad (5)$$

summing over all domain pair capacitances, including those with nearby domains on both the TM or sensor [31]. This combines with Eq. (4) to yield the charge-dependent force. For a centered TM, such that $\frac{\partial C_T}{\partial x} = 0$,

$$\frac{\partial F_x}{\partial q} \equiv \frac{-1}{C_T}\left|\frac{\partial C_X}{\partial x}\right|\Delta_x = \frac{-1}{C_T}\sum_{i(\mathrm{TM}),j(S)}\frac{\partial C_{ij}}{\partial x}(V_j - \delta V_i). \quad (6)$$

The derivative $\frac{\partial C_X}{\partial x}$ normalizes Δ_x to a single X electrode potential, such that $+V$ applied to electrode $X1+$ or $X2+$ increases Δ_x by V, with the opposite change obtained with $X1-$ or $X2-$. Equation (6) differs from the analogous formula in Ref. [25] as it includes the spatially varying TM potential.

Shear forces arise naturally in Eq. (5), in contrast with equipotential TM models [20,25], for which the relevant derivative in Eq. (5) becomes $\frac{\partial C_{Sj}}{\partial x}$. Nonzero for the gap-dependent capacitances of a sensor X-face domain, $\frac{\partial C_{Sj}}{\partial x}$ vanishes for a typical sensor Y or Z domain far from the TM edge, as TM motion along x gives fixed-gap sliding of a large conducting plane. With a patchwork TM surface, a sensor Y or Z domain "overlaps" with several opposing TM domains, giving $\frac{\partial C_{ij}}{\partial x} \neq 0$ and thus a force in the x direction. The field component along the underlying conducting TM surface vanishes, but its gradient does not, creating a shear force on the TM surface dipole distribution that generates the varying surface potential [21,32]. Stray torques from such shear forces limited sensitivity for the spherical Gravity Probe B gyroscopes [7].

Electrostatic shear is not essential to $\frac{\partial F_x}{\partial q}$ (see Ref. [33]); Δ_x reflects the average field along x felt by the TM free charge, and the uniform change in V_{TM} caused by q does not create significant field gradients that shear the TM surface dipoles. However, shear forces impact attempts to measure Δ_x with applied voltages and, thus, also the random charge problem.

Ideally, Δ_x is measured by the force caused by a change in TM charge, with voltages then applied to the X electrodes to null $\frac{\partial F_x}{\partial q}$. An easier proposed method [25] simulates charge by modulating V_{TM} with $V_0 \sin 2\pi f_0 t$ applied to the four Z electrodes. Combining Eqs. (4) and (5) yields the coherent force

$$F_{x(1f)} = -V_0 \sin 2\pi f_0 t \times \left\{\alpha_z\left|\frac{\partial C_X}{\partial x}\right|\Delta_x - \sum_{i(\mathrm{TM}),j(S_z)}\frac{\partial C_{ij}}{\partial x}(\delta V_j - \delta V_i)\right\}. \quad (7)$$

Here, $j(S_z)$ sums over domains on the modulated Z electrodes and $\alpha_z = 4C_Z/C_T \approx 0.07$. The first term is proportional to Δ_x, while the second, irrelevant to $\frac{\partial F_x}{\partial q}$, is the shear action of modulated field gradients near the Z electrodes on

nearby TM surface dipoles. It vanishes with an equipotential TM, with $\frac{\partial C_{Sj}}{\partial x} \approx 0$ for a Z-electrode domain j.

TM inclination with respect to the Z electrodes also introduces error, with a gap-varying $\frac{\partial C_Z}{\partial x}$ coupling the Z-electrode surface potentials and modulation voltage. However, shear coupling to the varying TM potential represents a more fundamental error that limits any technique to measure $\frac{\partial F_x}{\partial q}$ with applied voltages—without actually varying q—even with perfect alignment.

Experimentally, with a torsion pendulum sensitive to torque, N_ϕ (see Fig. 1), we assess Δ_x and its fluctuations by measuring the rotational imbalance Δ_ϕ relevant to $\frac{\partial N_\phi}{\partial q}$. Δ_ϕ is defined analogously to Δ_x [$x \rightarrow \phi$ in Eqs. (1), (6), and (7)]. With an equipotential TM and individually equipotential electrodes, Δ_x and Δ_ϕ become, respectively, the left-right and diagonal imbalances of the same four X-electrode potentials, $\Delta_x = (V_{X1+} + V_{X2+} - V_{X1-} - V_{X2-})$ and $\Delta_\phi = (V_{X1+} - V_{X2+} - V_{X1-} + V_{X2-})$ [25]. With electrostatically inhomogeneous conductors, Δ_ϕ has gap-varying sensitivity to the Y surface potentials as well as the X domains that dominate Δ_x [33] and, thus, statistically overestimates Δ_x and its fluctuations.

The Z-modulation measurement of Δ_ϕ is compared here with direct measurement of $\frac{\partial N_\phi}{\partial q}$ (see Fig. 3). Measurements are performed as a function of compensation voltage V_{COMP}, applied with positive (negative) polarity on the $X1+$ and $X2-$ ($X1-$ and $X2+$) electrodes. We measure $\frac{\partial N_\phi}{\partial q}$ by the change in torque, up to 5 fN m and measured to ± 0.1 fN m, upon rapid change in TM charge, of the order of $10^7 e$ caused by 10–30 s UV illuminations. The Z-modulation and charge measurement technique were applied and analyzed as in Refs. [16,25].

The uncompensated $\Delta_\phi \approx 38$ mV measured by charge variation is in the typical range of other sensors [16,17], and the slope of 4 confirms Eqs. (6) and (7) for four compensated X electrodes. The result for 4-electrode Z modulation, $\Delta_\phi \approx 51$ mV, is 13 mV larger. Additional tests with modulation on only the $Z+$ or $Z-$ electrode pairs give values of Δ_ϕ differing by more than 50 mV (Fig. 3), with a 90 mV range observed for Δ_ϕ with individual modulation of the four Z electrodes.

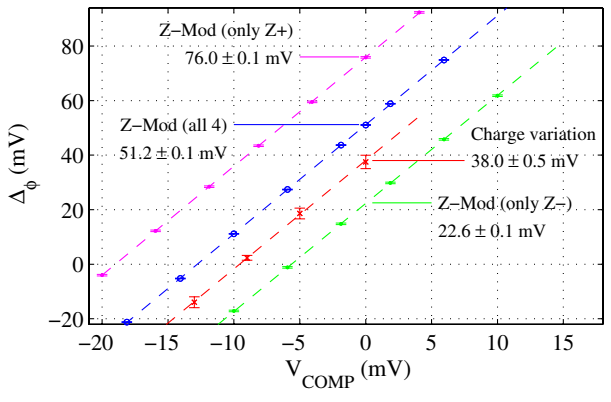

FIG. 3 (color online). Comparison of Δ_ϕ obtained by charge variation and by the Z-modulation technique, with extracted values for the uncompensated Δ_ϕ ($V_{\mathrm{COMP}} = 0$). Single point error bars (< 300 μV) are not visible in the modulation data.

The disagreement of the various Z-modulation results with Δ_ϕ measured with $\frac{\partial N_\phi}{\partial q}$ indicates the level of error in the Z-modulation technique. With an equipotential TM, these measurements should yield the same value. The variation between results with different Z electrodes reflects differences in the TM potentials near the different Z electrodes. This partially averages out by modulating all four Z electrodes but still leaves a significant 13 mV deviation from the true Δ_ϕ. For comparison and an indication of long term stability, the same sensor 1 yr before gave $\Delta_\phi \approx 135$ mV, with an 8 mV difference between the $\frac{\partial N_\phi}{\partial q}$ and Z-modulation techniques.

To limit the random charge contribution to the LISA acceleration noise (Fig. 6), we want $\Delta_x < 10$ mV. This will likely require in-flight measurement and compensation of intrinsic imbalances typically of the order of 100 mV, repeated periodically, given the slow drifts observed here and elsewhere [18]. Additionally, analysis and measurements indicate that errors associated with the Z-modulation technique may not allow 10 mV accuracy. This would require the more cumbersome direct measurement of $\frac{\partial F_x}{\partial q}$ in flight, which needs UV light actuation, charge measurements, and transient force detection.

Noise in Δ_x is assessed with two different measurements of S_{Δ_ϕ}. We first measure torque noise with a charged TM, attributing any excess to Δ_ϕ fluctuations,

$$S_N(q) - S_N(0) = \left[\frac{q}{C_T}\left|\frac{\partial C_X}{\partial \phi}\right|\right]^2 S_{\Delta_\phi}. \tag{8}$$

Measurements for 3 consecutive weekends with the TM charged to $V_{\mathrm{TM}} = 1.82 \pm 0.02$ V ($q \approx 4 \times 10^8 e$) were sandwiched between 4 weekends with the TM neutral to within 20 mV. The noise analysis, similar to Ref. [34], uses 25 000 s Blackman-Harris windows with 66% overlap—55 and 70 windows for, respectively, the charged and neutral TM data—binned into 8 frequencies per decade and averaged, with uncertainties based on standard deviation among preaveraged groups of 5 windows.

Figure 4 shows averaged torque noise, similar for the charged and neutral TM and with a minimum near 3 mHz of roughly 0.7 fN m/Hz$^{1/2}$ (120 μV/Hz$^{1/2}$). Following Eq. (8), we subtract the neutral TM background $S_N(0)$—measured to be stationary at the 0.1(fN m)^2/Hz level—to obtain S_{Δ_ϕ} in Fig. 5. The 1–4 mHz average is roughly 50 μV/Hz$^{1/2}$, resolved at nearly the 2σ level. Background noise and the associated errors bars increase at both higher and lower frequencies, with no resolvable excess.

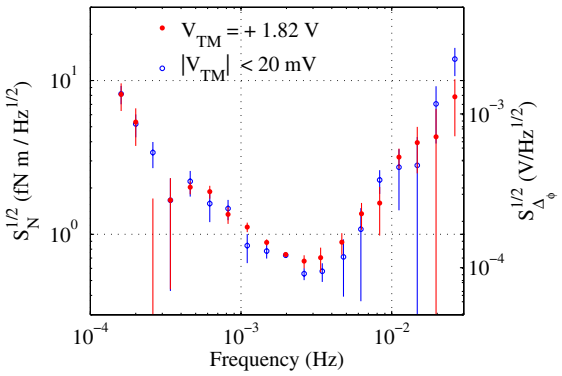

FIG. 4 (color online). Pendulum torque noise measured with the TM nearly neutral and when charged to a potential $V_{\mathrm{TM}} = +1.82$ V, with conversion into S_{Δ_ϕ} shown at right.

We also measure residual fluctuations in the Z-modulation signal, as in Ref. [17] and Eq. (7), with $\Delta_\phi(t)$ detected in the coherent torque amplitude at the modulation frequency f_0. This overestimates S_{Δ_ϕ} by the second term in Eq. (7) but improves sensitivity to low frequency fluctuations in Δ_ϕ, which are spectrally upshifted to amplitude modulate the torque carrier around $f_0 = 3$ mHz, chosen to minimize torque noise. V_{COMP} is adjusted to null the signal upon starting the measurement. $\Delta_\phi(t)$ is corrected for the measured dependence on tilt-induced TM translation inside the sensor. We subtract the background measurement noise, typically 500 $\mu\mathrm{V/Hz}^{1/2}$, as calculated with the demodulated quadrature (cosine) torque phase, which contains statistical torque noise without electrostatic signal. Spectra are calculated with 60 000 s windows, binned and averaged, and then background subtracted for each of 13 weekend measurements, with uncertainties based on scatter between different windows. Figure 5 shows a weighted mean of these data.

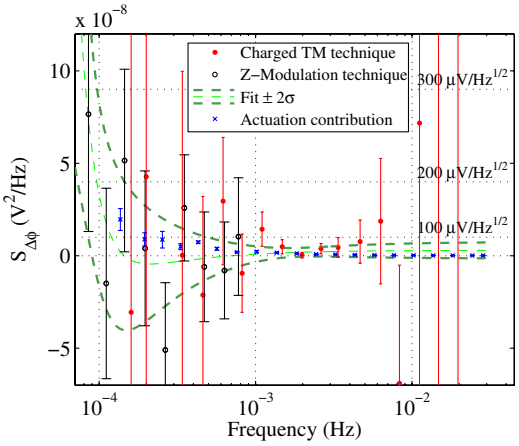

FIG. 5 (color online). Stray potential noise S_{Δ_ϕ}, measured with two techniques. Statistically insignificant large error points are omitted from each data set. Also shown are a fit to the joint data set and the noise contribution from the actuation electronics.

The measurements with a charged TM (•) and Z modulation (∘) combine in Fig. 5 [35] for a significant upper limit on the noise power S_{Δ_ϕ} from 0.1 to 5 mHz. We fit the combined data set to various models with a low frequency increase—Fig. 5 shows a fit with f^{-1} and f^{-4} terms—and find 2σ confidence intervals of (0, 80) $\mu\mathrm{V/Hz}^{1/2}$ at 1 mHz and (0, 290) $\mu\mathrm{V/Hz}^{1/2}$ at 0.1 mHz. Also shown (×) is the contribution from the four X-electrode actuation circuits [36], measured separately to give f^{-1} noise power with roughly 50 $\mu\mathrm{V/Hz}^{1/2}$ at 1 mHz. The weakly detected fluctuations are thus consistent with electronic noise, and we do not resolve true surface potential fluctuations in the LISA bandwidth. Δ_ϕ effectively sums the noise of many (≈ 16; see Ref. [33]) areas the size of a LISA X electrode (≈ 500 mm^2), and, for fluctuations that are uncorrelated on larger spatial scales, our 2σ upper limit corresponds to 12 $\mu\mathrm{V/Hz}^{1/2}$ in the average potential difference between 500 mm^2 surface regions.

The $+2\sigma$ curve in Fig. 5 is taken as an upper limit for S_{Δ_x} in the acceleration noise budget in Fig. 6. Assuming a TM charge of $10^7 e$, this result is compatible with the LISA goals, marginally so at 0.1 mHz. This significantly improves upon previous upper limits with LISA prototype hardware, from roughly 1 $\mathrm{mV/Hz}^{1/2}$ [17] to 80 $\mu\mathrm{V/Hz}^{1/2}$ at 1 mHz. The limit is also below the 150–200 $\mu\mathrm{V/Hz}^{1/2}$ deduced for $S_{\Delta_x}^{1/2}$ at 1 mHz from observations of potential fluctuations between opposing gold-coated plates [18,33].

Several design aspects merit consideration for improving upon the noise budget in Fig. 6. A thin ground wire can eliminate TM charge [4,37] but introduces thermal mechanical noise well beyond the $(\mathrm{fm/s}^2)/\mathrm{Hz}^{1/2}$ level [38]. With a floating TM, the q-δV interaction has roughly d^{-1} dependence [Eq. (1)]. Larger gaps help, but even a factor of 10, $d = 4$ cm, will lower the random charge noise in Fig. 6 only if $\Delta_x < 100$ mV, which may still require voltage-controlled electrodes for compensation. This introduces actuation circuitry noise, which sums with, or even dominates over, surface potential fluctuations. Preliminary measurements for the LISA Pathfinder electronics indicate a circuit contribution $S_{\Delta_x}^{1/2} \approx 30$ $\mu\mathrm{V/Hz}^{1/2}$ [39].

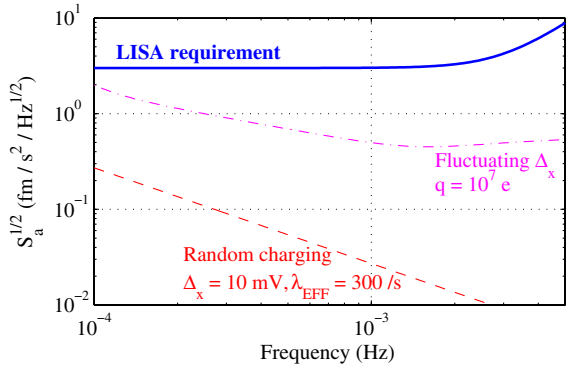

FIG. 6 (color online). Conservative acceleration noise budget for the $q - \delta V$ interaction, with (bold) the LISA goal.

Along with the interaction with TM charge, stray potential fluctuations can also create force noise by mixing with stable domain potentials, even with $q = 0$, as allowed by Eq. (5). Analysis of this effect demands combining averaged potential fluctuation data with the domain spatial distribution and correlations. This will impact in-flight operation issues such as the extent to which continuous TM discharge can reduce noise.

This work was supported by the Istituto Nazionale di Fisica Nucleare, the Agenzia Spaziale Italiana (LISA Pathfinder contract), and the Italian Ministry of University and Research (PRIN 2008).

[1] D. Ugolini, R. McKinney, and G. M. Harry, Rev. Sci. Instrum. **78**, 046102 (2007).
[2] M. Hewitson, K. Danzmann, H. Grote, S. Hild, J. Hough, H. Lück, S. Rowan, J. R. Smith, K. A. Strain, and B. Willke, Classical Quantum Gravity **24**, 6379 (2007).
[3] P. Bender *et al.*, LISA Report No. ESA-SCI(2000)11, 2000.
[4] R. Chhun, D. Hudson, P. Flinoise, M. Rodrigues, P. Touboul, and B. Foulon, Acta Astronaut. **60**, 873 (2007).
[5] D. J. Kapner, T. S. Cook, E. G. Adelberger, J. H. Gundlach, B. R. Heckel, C. D. Hoyle, and H. E. Swanson, Phys. Rev. Lett. **98**, 021101 (2007).
[6] J. C. Long, H. W. Chan, A. B. Churnside, E. A. Gulbis, M. C. M. Varney, and J. C. Price, Nature (London) **421**, 922 (2003).
[7] C. W. F. Everitt *et al.*, Phys. Rev. Lett. **106**, 221101 (2011).
[8] S. Buchman and J. Turneaure, Rev. Sci. Instrum. **82**, 074502 (2011).
[9] M. Armano *et al.*, Classical Quantum Gravity **26**, 094001 (2009).
[10] F. Antonucci *et al.*, Classical Quantum Gravity **28**, 094002 (2011).
[11] R. Dolesi *et al.*, Classical Quantum Gravity **20**, S99 (2003).
[12] W. J. Weber, D. Bortoluzzi, A. Cavalleri, L. Carbone, M. Da Lio, R. Dolesi, G. Fontana, C. D. Hoyle, M. Hueller, and S. Vitale, Proc. SPIE Int. Soc. Opt. Eng. **4856**, 31 (2002).
[13] H. M. Araùjo, P. Wass, D. Shaul, G. Rochester, and T. J. Sumner, Astropart. Phys. **22**, 451 (2005).
[14] J. B. Camp, T. W. Darling, and R. E. Brown, J. Appl. Phys. **69**, 7126 (1991).
[15] C. C. Speake and C. Trenkel, Phys. Rev. Lett. **90**, 160403 (2003).
[16] L. Carbone, A. Cavalleri, R. Dolesi, C. D. Hoyle, M. Hueller, S. Vitale, and W. J. Weber, Phys. Rev. Lett. **91**, 151101 (2003).
[17] L. Carbone, A. Cavalleri, R. Dolesi, C. D. Hoyle, M. Hueller, S. Vitale, and W. J. Weber, Classical Quantum Gravity **22**, S509 (2005).
[18] S. E. Pollack, S. Schlamminger, and J. H. Gundlach, Phys. Rev. Lett. **101**, 071101 (2008).
[19] N. A. Robertson, J. R. Blackwood, S. Buchman, R. L. Byer, J. Camp, D. Gill, J. Hanson, S. Williams, and P. Zhou, Classical Quantum Gravity **23**, 2665 (2006).
[20] D. A. S. Shaul, H. M. Araújo, G. K. Rochester, T. J. Sumner, and P. J. Wass, Classical Quantum Gravity **22**, S297 (2005).
[21] C. C. Speake, Classical Quantum Gravity **13**, A291 (1996).
[22] B. Schumaker, Classical Quantum Gravity **20**, S239 (2003).
[23] R. T. Stebbins, P. L. Bender, J. Hanson, C. D. Hoyle, B. L. Schumaker, and S. Vitale, Classical Quantum Gravity **21**, S653 (2004).
[24] P. L. Bender, Classical Quantum Gravity **20**, S301 (2003).
[25] W. J. Weber, L. Carbone, A. Cavalleri, R. Dolesi, C. D. Hoyle, M. Hueller, and S. Vitale, Adv. Space Res. **39**, 213 (2007).
[26] A. Cavalleri, G. Ciani, R. Dolesi, M. Hueller, D. Nicolodi, D. Tombolato, P. J. Wass, W. J. Weber, S. Vitale, and L. Carbone, Classical Quantum Gravity **26**, 094012 (2009).
[27] H. Vocca *et al.*, Classical Quantum Gravity **21**, S665 (2004).
[28] This is equivalent to the capacitive matrix formulation, with $q_i = \sum_j c_{ij} V_j$ and energy $U = \frac{1}{2}\sum_{i,j} c_{ij} V_i V_j$. The symmetries imposed by the Laplace equation [29] allow the electrical circuit analogy, with $c_{ij} = c_{ji} = -C_{ij}$ for $j \neq i$ and $c_{ii} = \sum_{j \neq i} C_{ij}$. From this, Eq. (5) follows.
[29] W. J. Herrera and R. A. Diaz, Am. J. Phys. **76**, 55 (2008).
[30] We choose the convention $\sum_{i(\mathrm{TM}),j(S)} C_{ij} \delta V_i = 0$, such that $V_{\mathrm{TM}} = 0$ when $q = 0$ and all sensor domains are grounded, $V_{Sj} = 0$.
[31] N. Brandt and W. Fichter, J. Phys. Conf. Ser. **154**, 012008 (2009).
[32] J. D. Jackson, *Classical Electrodynamics* (Wiley, New York, 1975).
[33] See Supplemental Material at http://link.aps.org/supplemental/10.1103/PhysRevLett.108.181101 for a discussion of the stray potentials that dominate Δ_x and an approximate model for comparing stray potential measurements in different geometries.
[34] A. Cavalleri *et al.*, Classical Quantum Gravity **26**, 094017 (2009).
[35] For both measurements, the estimated noise power excess S_{Δ_ϕ} is in many cases smaller than the measurement uncertainty, and so negative data points are statistically inevitable. These negative data do not allow a conventional log-scale plot of linear spectral density $S_{\Delta_\phi}^{1/2}$ and force a linear plot of the power spectral density. Key linear spectral levels like 100 $\mu\mathrm{V}/\mathrm{Hz}^{1/2}$ are shown as a guide.
[36] The actuation noise, measured with a chopper-demodulation technique, comes from commercial digital-to-analog converter (NI-6703) and instrumentation amplifier (AD-622) components.
[37] P. Touboul, B. Foulon, M. Rodrigues, and J. P. Marque, Aerospace Sci. Technol. **8**, 431 (2004).
[38] E. Willemot and P. Touboul, Rev. Sci. Instrum. **71**, 302 (2000).
[39] C. Praplan, HEV-SO Valais Technical Report S2-HEV-RP3042, LISA Pathfinder, 2009.